Optically imprinted reconfigurable photonic elements in a VO2 nanocomposite

Thorben Jostmeier, Johannes Zimmer, Helmut Karl, Hubert J. Krenner, Markus Betz

Angaben zur Veröffentlichung / Publication details:

Jostmeier, Thorben, Johannes Zimmer, Helmut Karl, Hubert J. Krenner, and Markus Betz. 2014. "Optically imprinted reconfigurable photonic elements in a VO2 nanocomposite." *Applied Physics Letters* 105 (7): 071107. https://doi.org/10.1063/1.4893570.

Applied Physics Letters

Optically imprinted reconfigurable photonic elements in a VO_2 nanocomposite

Cite as: Appl. Phys. Lett. **105**, 071107 (2014); https://doi.org/10.1063/1.4893570
Submitted: 06 July 2014 . Accepted: 07 August 2014 . Published Online: 21 August 2014

Thorben Jostmeier, Johannes Zimmer, Helmut Karl, Hubert J. Krenner, and Markus Betz

Optically imprinted reconfigurable photonic elements in a VO_2 nanocomposite

Thorben Jostmeier,[1] Johannes Zimmer,[2,3] Helmut Karl,[4] Hubert J. Krenner,[2,3] and Markus Betz[1]
[1]*Experimentelle Physik 2, TU Dortmund University, Otto-Hahn-Straße 4, 44227 Dortmund, Germany*
[2]*Lehrstuhl für Experimentalphysik 1 and Augsburg Centre for Innovative Technologies (ACIT), Universität Augsburg, Universitätstr. 1, 86159 Augsburg, Germany*
[3]*Nanosystems Initiative Munich (NIM), Schellingstr. 4, 80799 München, Germany*
[4]*Lehrstuhl für Experimentalphysik IV, Universität Augsburg, Universitätstr. 1, 86159 Augsburg, Germany*

(Received 6 July 2014; accepted 7 August 2014; published online 21 August 2014)

We investigate the optical and thermal hysteresis of single-domain vanadium dioxide nanocrystals fabricated by ion beam synthesis in a fused silica matrix. The nanocrystals exhibit a giant hysteresis, which permits to optically generate a long-time stable supercooled metallic phase persistent down to practically room temperature. Spatial patterns of supercooled and insulating nanocrystals feature a large dielectric contrast, in particular, for telecom wavelengths. We utilize this contrast to optically imprint reconfigurable photonic elements comprising diffraction gratings as well as on- and off-axis zone plates. The structures allow for highly repetitive ($>10^4$) cycling through the phase transition without structural damage. © *2014 AIP Publishing LLC*.
[http://dx.doi.org/10.1063/1.4893570]

Vanadium dioxide (VO_2) has attracted the interest of researchers for decades since it exhibits a metal-insulator phase transition (MIT) near ambient temperatures ($T_C \approx 68\,^\circ$C in bulk crystals). Upon heating, VO_2 undergoes a structural and electronic change from a room temperature insulating phase to a high temperature metallic phase. This phase transition is accompanied by a change of the DC electrical conductivity by five orders of magnitude and a substantial modification of the complex dielectric function.[1,2] Closely related, the metallic phase features decreased transmission for near-infrared (NIR) radiation. For nanoscopic VO_2, the MIT shows a thermal hysteresis such that a supercooled metallic state can persist to temperatures somewhat below T_C.[2–4] The MIT in VO_2 can be also induced optically on sub-picosecond timescales.[5,6] Recent studies performed on bulk-like polycrystalline films have elucidated the microscopic details of this ultrafast phase transition.[7] VO_2 based structures are envisioned for applications such as switchable optical elements[8,9] and optically controlling the phase of light.[10] As an example, it has been shown that the dielectric contrast between insulating and metallic phases of VO_2-nanocrystals (NCs) in a fused silica matrix defines nanothermochromic diffraction gratings.[11] In this approach, site-selective bombardment with argon ions introduces defects into sub-ensembles of the nanocrystals which inhibit the MIT. The resulting dielectric contrast for temperatures below and above T_C allows for the implementation of switchable, large-contrast diffraction gratings at telecom wavelengths.

The goal of the present work is to extend this approach and optically imprint long-term stable dielectric patterns into an otherwise unstructured sample containing a dense layer of VO_2-NCs. As a first step, we investigate the optical hysteresis and bistability of the NCs. We then move on to utilize their broad thermal and optical hysteresis to define micropatterns of insulating and supercooled metallic NCs. These structures serve as photonic elements for telecom wavelengths. As fundamental paradigms, we imprint diffraction gratings and optical zone plates. While such photonic elements are stable close to room temperature, they can be fully erased by cooling the structure to $\sim$10 °C below ambient values. Remarkably, the NC samples permit highly repetitive non-destructive cycling through the phase transition.

Our samples consist of VO_2-NCs embedded into a 0.5 mm thick fused silica matrix. The NCs are synthesized by sequential ion beam implantation of vanadium ($9 \times 10^{16}\,\frac{\text{at}}{\text{cm}^2}$ at 100 keV) and oxygen ($1.8 \times 10^{17}\,\frac{\text{at}}{\text{cm}^2}$ at 36 keV).[4,11] In a subsequent 10 min rapid thermal annealing step at 1000 °C, the VO_2-NCs are formed. They are centered 85 nm below the sample surface with an average diameter of 90 nm and a similar average lateral spacing (areal density $\sim 1 \times 10^{10}\,\text{cm}^{-2}$). A typical transmission electron micrograph is shown in Fig. 1(a). The samples are located on a temperature-controlled mount in order to precisely define their overall lattice temperature. We use an all-optical approach to locally induce and monitor the MIT of the VO_2-NCs nanocomposit. A cw 532 nm pump laser locally induces the MIT on a μm-scale. It mainly deposits heat and, thereby, locally raises the lattice temperature above the transition temperature. The duration of the illumination can be precisely adjusted with a fast mechanical shutter. A low-power cw laser at 1.55 μm wavelength probes the momentary phase of the NCs. In particular, we spatially resolve the normal-incidence optical transmission trough the VO_2-NC layer, which differs by $\sim$20% between the insulating and metallic state of the NCs.

We begin the characterization of the MIT in our NCs by analyzing their thermal hysteresis. As displayed in Fig. 1(b), the optical transmission at 1.55 μm features a sharp decrease above a critical temperature of $T_C \approx 80\,^\circ$C. This finding mirrors the enhanced NIR absorption of the metallic phase which leads to a 20% reduction of the optical transmission even though the effective interaction length is $<$50 nm. This increased absorption is also confirmed by spectral ellipsometry, which evidences five-fold increase of the imaginary part

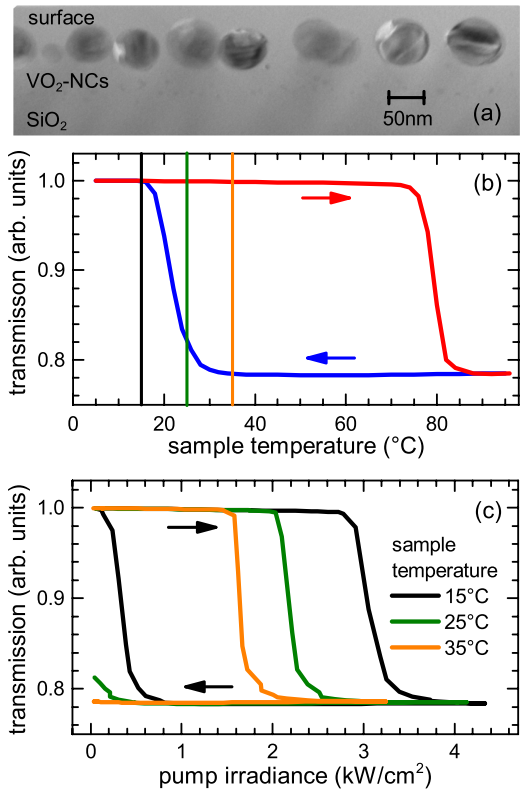

FIG. 1. (a) Cross-section transmission electron microscope image of ion beam synthesized VO_2 nanocrystals embedded in a fused silica matrix. (b) Thermal hysteresis recorded by tracking the 1.55 μm probe transmission for increasing (red) and decreasing (blue) sample temperatures. The vertical lines indicate the temperatures used for the analysis of the optical hysteresis in panel (c). (c) Optically induced phase transition and hysteresis for different sample temperatures. Arrows indicate increasing and decreasing optical irradiances.

of the refractive index when compared to the insulating phase. Upon cooling, an extremely pronounced thermal hysteresis with a supercooled metallic state persistent down to practically room temperature is seen. The width of this thermal hysteresis clearly exceeds that of other nanoscale VO_2 systems reported so far.[13,14,16] This substantial bistability can be mainly attributed to two effects: (i) Our NCs have a relatively small volume and single-domain character with very few defects. The related absence of nucleation sites hampers the structural phase transition. As a result, the small NC volume and good crystal quality results in a higher critical temperature T_C and a lower back-switching temperature upon cooling. Studies of the dependences of the MIT and its hysteresis on size[12–15] and crystallinity[15,16] of nanoscale VO_2 support this interpretation. (ii) Embedding VO_2-NCs into a fused silica matrix induces local strain fields and pins the NCs. It has been shown that such a matrix changes the hysteresis of the MIT significantly.[17–19]

We now turn towards the investigation of the optically induced MIT and its hysteresis seen for increasing and decreasing 532 nm cw irradiances. The diameter of the probe beam is chosen less then half of the pump beam diameter ($\approx$100 μm FWHM) such that the probed NCs are illuminated with nearly homogeneous pump irradiance. After every change of the pump irradiance, the formation of a thermal equilibrium in the illuminated area is ensured. As depicted in Fig. 1(c), we find a remarkably broad and fully reversible hysteresis/bistability in this optically induced MIT. Its shape resembles the thermally induced one. Remarkably, for lattice temperatures slightly above ambient values the optically prepared metallic phase persists even without any further illumination. In essence, the very pronounced hysteresis completely inhibits the NCs from undergoing the reverse MIT into the insulating state for lattice temperatures above $\approx$35 °C. In addition, the threshold irradiance required to induce the MIT is reduced for larger lattice temperatures, as is intuitively expected.

Taken together, the pronounced optical and thermal hysteresis of the VO_2-NCs allows for a simple preparation of a persistent stable supercooled metallic phase using optical excitation. We have explicitly verified the long-term stability of the optically generated supercooled state at a lattice temperature of $T = 40$ °C (data not shown). The supercooled state persists for several hours without any noticeable relaxation. However, cooling down the sample to $T < 15$ °C immediately induces the reverse MIT and resets all NCs into the insulating state.

The approach to optically define supercooled VO_2-NCs puts us in a position to almost arbitrarily define planar photonic micropatterns in an otherwise unstructured sample by local control with focused laser radiation. More specifically, the laser acts as a source of rapid thermal processing to induce the MIT. As a first example, we imprint a grating structure by interfering two 532 nm cw pump beams incident for 1 ms on the NC layer kept at 40 °C. The two pump beams impinge with a relative angle of $\sim$3° and give rise to an interference pattern of 15 μm period (cf. Figs. 2(a) and 2(b)). This spatially periodic, short-term heat deposition results in a corresponding pattern of insulating and supercooled metallic VO_2-NCs. Owing to their different complex dielectric functions, the structure acts as a diffraction grating for telecom

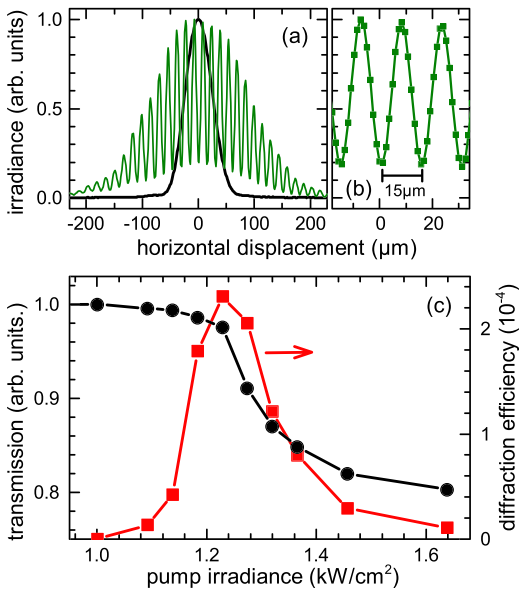

FIG. 2. (a) Horizontal scans of the spatial irradiance profile of 532 nm pump (green) and 1.55 μm probe (black) beams, recorded with a rotating-slit beam profiler. The pump configuration is achieved by two tilted pump beams interfering on the sample. (b) Close-up of the central part of the pump spot demonstrating the interference contrast. (c) Pump power dependence of the transmission (black) and first order diffraction (red) of 1.55 μm light interacting with the optically imprinted grating of 15 μm period.

radiation. Again, the probe beam is focused to the center of this pattern to ensure the interaction with a homogeneously illuminated section of the optically imprinted photonic structure. Using a germanium photodiode, we measure the first order diffracted intensity of the probe beam. In Fig. 2(c), we present data for the transmission and first order diffraction as a function of the irradiance of a pump pulse pair of 1 ms duration. We find only a small window of pump irradiances that provides the proper amount of heating to trigger the MIT while still preventing heat diffusion from switching the entire illuminated area. Specifically, for insufficient or excessive pump irradiances, the entire illumination spot remains insulating or switches to the metallic phase, respectively. This finding is corroborated by the respective data for the transmissivity seen in Fig. 2(c). The peak diffraction efficiency does not exceed 2×10^{-4}. This value points to a limited dielectric contrast that is achieved by this one-shot approach with two interfering large-area excitation beams. Apparently, for such a configuration in-plane heat diffusion inhibits a fully modulated pattern of insulating/metallic NCs. We note that somewhat other combinations of the irradiance and duration of the illumination do not increase the diffraction efficiency.

In order to improve the dielectric contrast and to be able to define more complex photonic patterns, we now turn towards a point-by-point inscription of the MIT with tightly focused optical beams. To this end, the sample is mounted on a 2D motorized translation stage with sub-μm accuracy. An aspheric lens focuses the 532 nm pump light down to a $\sim$5 μm excitation spot. The area undergoing the optically induced MIT can, in principle, be reduced even below the optical spot size: As the behavior of the MIT is strongly nonlinear, the pump power can be adjusted such that only the NCs in the center section of the Gaussian profile are heated sufficiently strong to undergo the MIT. In the present configuration, 10 mW pump pulses of ms duration are capable of locally driving the MIT such that low-cost laser diodes are sufficient to rapidly imprint dielectric patterns. The inset in Fig. 3 shows a 2D transmissivity map of a grating of 20 μm periodicity generated by such a point-by-point definition. During the definition of the grating, the sample is kept at 40 °C. As seen in Fig. 3, the grating features a first-order diffraction efficiency of 1.6×10^{-3}, i.e., about an order of magnitude larger when compared to an inscription with interfering large-area pump beams discussed above. The imprinted dielectric patterns are long-term stable at 40 °C. As evident from Fig. 3, it can be easily erased in a non-destructive fashion by cooling down the sample to slightly below room temperature. The maximum diffraction efficiency of 1.6×10^{-3} is already very similar to those achieved with pre-defined full-contrast gratings reported in Ref. 11. From this agreement, we conclude that the optically generated micropatterns succeed in attaining the maximum possible dielectric contrast in the present VO_2-NCs samples. Apparently, inducing the MIT with tightly confined optical beams leads to much less heat dissipation to the surrounding areas when compared to the above situation of interfering large-area beams.

The method of point-by-point inscription of dielectric patterns with μm-resolution permits to create more sophisticated planar dielectric patterns of alternating insulating and metallic VO_2-NCs. As an example, we define on- and off-axis zone plates which are visualized in the transmissivity maps in Figs. 4(a) and 4(c). To generate these structures, we move the sample with an in-plane velocity of $1\,\frac{\mu m}{ms}$, while a continuous 532 nm, 10 mW pump spot of 5 μm diameter induces the MIT. In general, a zone plate consists of concentric circles of areas with different refractive index or transmission. More specifically, the radius of the m-th circle scales as $r_m \approx \sqrt{mf\lambda}$. The example in Fig. 4(a) represents

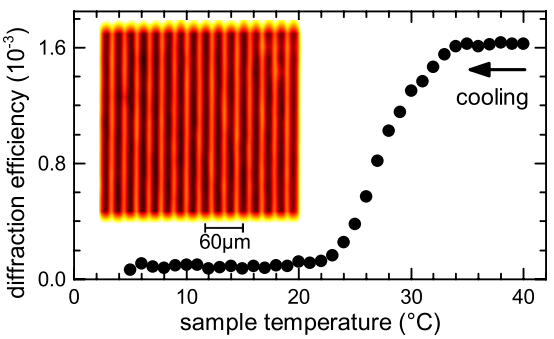

FIG. 3. Temperature dependence of the diffraction efficiency of a grating pattern formed from insulating and metallic VO_2-NCs. The pattern is optically defined point-by-point at a lattice temperature of 40 °C. After the preparation of the grating the sample is cooled down to 5 °C, where the insulating state is fully recovered. The inset shows a transmissivity map of the sample. The optical contrast relies on the different absorption of metallic and insulating NCs.

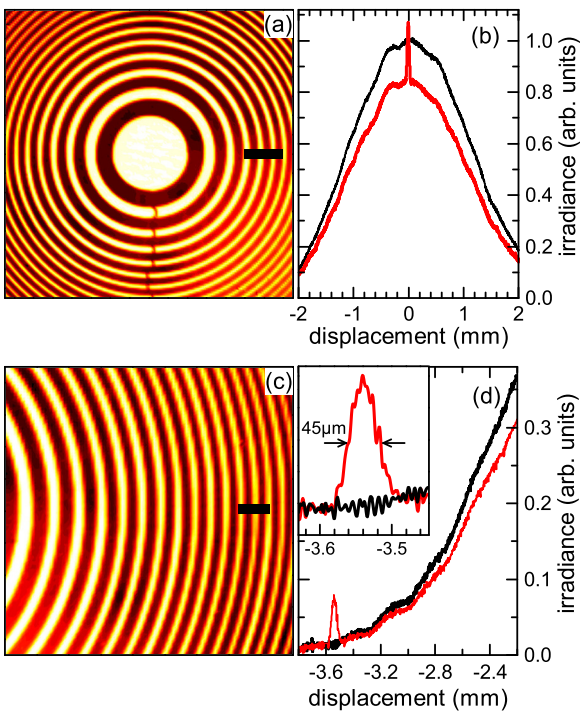

FIG. 4. (a) Transmissivity map of an on-axis zone plate defined by an optically imprinted pattern of insulating and metallic VO_2-NCs (sample temperature 40 °C). The scale bar is 400 μm. (b) Cross-section of the optical beam in the focal plane of the on-axis zone plate before (black) and after (red) optical imprinting of the zone plate. (c) Transmissivity map of an off-axis zone plate. The scale bar is 200 μm. (d) Cross-section of the optical beam in the focal plane of the off-axis zone plate before (black) and after (red) optical imprinting of the zone plate. The inset shows the focal spot generated by the off-axis zone plate.

an on-axis zone plate with $f = 10\,\text{cm}$ focal lengths for $\lambda = 1.55\,\mu m$ radiation. To verify the functionality of this zone plate, it is illuminated with a non-focused $1.55\,\mu\text{m}$ probe beam. Fig. 4(b) shows the spatial profile recorded at 10 cm behind the sample plane with (red) and without (black) the optically imprinted dielectric pattern. Upon definition of the dielectric pattern, the overall transmission decreases by ~15%. This is expected because ~50% of the NCs are now in the metallic state. In addition, the zone plate creates a focal spot in the center of the beam profile. The local light intensity is enhanced and exceeds the intensity measured without an imprinted zone plate. We extend this concept and also realize an off-axis zone plate. The corresponding results are shown in Figs. 4(c) and 4(d). Remarkably, a part of the $1.55\,\mu\text{m}$ light is now focused to a $\sim 45\,\mu\text{m}$ spot outside the transmitted beam.

The present optical approach also permits to explore the limits of highly repetitive switching of the MIT. Most potential applications aiming to utilize the phase transition in VO_2 require a fully reversible, non-destructive MIT. Bulk and thin-film VO_2 specimens, however, often suffer from structural disintegration when repetitively undergoing the MIT. The high crystal quality of our VO_2-NCs and the surrounding fused silica matrix resolve this detrimental limitation.[18] To verify that stability, we apply a 1 Hz modulation to the 532 nm pump laser such that the NCs recover to the insulating state after each excitation event which takes place at a sample temperature of 10 °C. We then monitor the $1.55\,\mu\text{m}$ transmission of the excitation spot. Remarkably, we do not see any degradation effects in the MIT of the VO_2-NCs even after $>10^4$ cycles between insulating and metallic phases.

In conclusion, we have realized reconfigurable optical elements formed from spatial micro-patterns of insulating and supercooled VO_2-NCs. The definition of the functional structures occurs optically and the erasing of the optical elements is achieved by cooling to below room temperature. While the present study focuses on planar optical elements, more complex structures can be realized in samples containing several layers of NCs. The hysteresis underlying our concept allows for the switching into a persistent supercooled metallic phase and can probably be further enlarged by defining smaller NCs.

We thank E. Sternemann for helpful discussions. H.J.K. acknowledges support of the DFG through the Emmy-Noether program.

[1]F. J. Morin, Phys. Rev. Lett. **3**, 34–36 (1959).
[2]H. W. Verleur, A. S. Barker, Jr., and C. N. Berglund, Phys. Rev. **172**, 788–798 (1968).
[3]W. R. Roach, Appl. Phys. Lett. **19**, 453–455 (1971).
[4]R. Lopez, L. A. Boatner, T. E. Haynes, L. C. Feldman, and R. F. Haglund, Jr., J. Appl. Phys. **92**, 4031–4036 (2002).
[5]M. F. Becker, A. B. Buckman, R. M. Walser, T. Lépine, P. Georges, and A. Brun, J. Appl. Phys. **79**, 2404–2408 (1996).
[6]A. Cavalleri, Cs. Tóth, C. W. Siders, J. A. Squier, F. Ráksi, P. Forget, and J. C. Kieffer, Phys. Rev. Lett. **87**, 237401 (2001).
[7]A. Pashkin, C. Kübler, H. Ehrke, R. Lopez, A. Halabica, R. F. Haglund, Jr., R. Huber, and A. Leitenstorfer, Phys. Rev. B **83**, 195120 (2011).
[8]S. B. Choi, J. S. Kyoung, H. S. Kim, H. R. Park, D. J. Park, B.-J. Kim, Y. H. Ahn, F. Rotermund, H.-T. Kim, K. J. Ahn, and D. S. Kim, Appl. Phys. Lett. **98**, 071105 (2011).
[9]G. Seo, B.-J. Kim, Y. W. Lee, and H.-T. Kim, Appl. Phys. Lett. **100**, 011908 (2012).
[10]T. V. Son, K. Zongo, C. Ba, G. Beydaghyan, and A. Haché, Opt. Commun. **320**, 151–155 (2014).
[11]J. Zimmer, A. Wixforth, H. Karl, and H. J. Krenner, Appl. Phys. Lett. **100**, 231911 (2012).
[12]R. Lopez, L. C. Feldman, and R. F. Haglund, Jr., Phys. Rev. Lett. **93**, 177403 (2004).
[13]K. Appavoo, D. Y. Lei, Y. Sonnefraud, B. Wang, S. T. Pantelides, S. A. Maier, and R. F. Haglund, Jr., Nano Lett. **12**, 780–786 (2012).
[14]H. Zhang, Z. Wu, X. Wu, W. Yang, and Y. Jiang, Vacuum **104**, 47–50 (2014).
[15]J. Y. Suh, R. Lopez, L. C. Feldman, and R. F. Haglund, Jr., J. Appl. Phys. **96**, 1209–1213 (2004).
[16]E. U. Donev, R. Lopez, L. C. Feldman, and R. F. Haglund, Jr., Nano Lett. **9**, 702–706 (2009).
[17]J. Wei, Z. Wang, W. Chen, and D. H. Cobden, Nat. Nanotechnol. **4**, 420–424 (2009).
[18]J. Cao, Y. Gu, W. Fan, L. Q. Chen, D. F. Ogletree, K. Chen, N. Tamura, M. Kunz, C. Barret, J. Seidel, and J. Wu, Nano Lett. **10**, 2667–2673 (2010).
[19]J. M. Atkin, S. Berweger, E. K. Chavez, M. B. Raschke, J. Cao, W. Fan, and J. Wu, Phys. Rev. B **85**, 020101 (2012).